Spatio-temporal filling of missing data in remotely sensed displacement measurement time series

Alexandre Hippert-Ferrer *, *Student Member, IEEE*, Yajing Yan *, *Member, IEEE*, Philippe Bolon *, *Senior Member, IEEE*, Romain Millan [†]

*LISTIC, Université Savoie Mont-Blanc, Annecy, France [†]IGE, Université Grenoble Alpes, Grenoble, France
Correspondence: alexandre.hippert-ferrer@univ-smb.fr

Abstract—Missing data is a critical pitfall in the investigation of remotely sensed displacement measurement, because it prevents from a full understanding of the physical phenomenon under observation. In the sight of reconstructing incomplete displacement data, this paper presents a data-driven spatio-temporal gap-filling method, which is an extension of the Expectation Maximization-Empirical Orthogonal Functions (EM-EOF) method. The presented method decomposes an augmented spatio-temporal covariance of a displacement time series into empirical orthogonal function (EOF) modes and then selects the optimal set of EOF modes to reconstruct the time series. This selection is based on the cross-validation root-mean-square error and a confidence index associated with each eigenvalue. The estimated missing values are then iteratively updated until convergence. Results on displacement time series derived from cross-correlation of Sentinel-2 optical images over Fox Glacier in New-Zealand's Alps show that the reconstruction accuracy is improved compared to the EM-EOF method. The proposed extension can tackle challenging cases, i.e. short time series with heterogeneous displacement behaviors corrupted by large amount of missing data and noise.

Index Terms—Gap-filling, covariance, EOF, displacement time series.

I. INTRODUCTION

The analysis of Earth's surface displacement is a thriving subject in remote sensing. In recent years, remotely sensed measurements of surface displacement have been significantly improved with new advanced multi-temporal methods [1], [2]. Despite this breakthrough, displacement time series are often subject to missing data in space and time dimensions. Data incompleteness is mainly due to technical limitations of the displacement computation methods (e.g. cross-correlation, differential interferometry) and/or surface property changes of the observed target. Such incompleteness is critical in earth sciences because it can impair the complete understanding of physical processes such as glacier sliding or crustal deformation. An accurate and efficient missing data reconstruction method, operating in both space and time, is thus needed to improve data completeness and reduce data uncertainty for remote sensing applications.

However, missing data in remotely sensed displacement measurement has not been drawn significant attention. Existing methods, e.g. Kriging, regression analysis, or spline interpolation are mainly focused on spatial or temporal interpolation only, which limits the use of the full spatio-temporal information [3]. Very recently, [4] proposed a method called EM-EOF

(Expectation Maximization-Empirical Orthogonal Functions), based on the EOF analysis of the temporal covariance of a displacement time series for missing data reconstruction. This technique iteratively decomposes the temporal covariance of the time series and estimates the optimal number of EOF modes to reconstruct the data, i.e. fills in the gaps and extracts significant trends from noisy data [5]. Promising results were obtained with time series of incomplete Sentinel-1 InSAR displacement measurement over Alpine glaciers. However, the EM-EOF method may present some limitations when i) the time series is small in length, ii) spatial correlation of the ground displacement field prevails overs temporal correlation and iii) the displacement field contains heterogeneous and local spatial features. In particular, as EM-EOF uses temporal covariance decomposition, reconstruction biases may arise when a pixel is never observed through the time series. These motivate us to employ the spatio-temporal covariance of the time series in order to take both temporal and spatial correlation of the displacement field into account.

For this, it is possible to augment the data by including lagged copies of itself in a larger sequence of data. Methods such as multivariate singular spectrum analysis (M-SSA) [6] use time lagged information to form an augmented covariance matrix and find propagating or periodic signals [7]. M-SSA has proven to be a good parametric-free method to decompose geophysical signals into separate components (e.g. trends, oscillations and noise) and to impute missing values [8], [9]. However, it is not particularly adapted to short time series with large spatial dimension. In [10], an implementation of SSA was extended to a single 2D image. This method operates first by a spatial augmentation of the data matrix into a Hankel-block-Hankel (HbH) matrix. Then, a low-rank approximation is performed from the singular value decomposition (SVD) of the data covariance. In the case of time series of 2D images, significant adaptations are still necessary for spatio-temporal covariance estimation.

The aim of this paper is to introduce an extension to the EM-EOF method (called extended EM-EOF hereafter): spatial lagged information is used to augment a time series of 2D displacement fields, which extends the principle of 2D-SSA to time series of 2D images. Because of the specific structure of the lagged spatio-temporal covariance, the direct link between the EOF modes and the physical interpretation is not obvious: a novel criterion, issued from a correlation-based uncertainty analysis of the eigenvalues, is proposed for selecting the

optimal sets of EOF modes. An approximation of the spatial lag range is also provided using a correlation-based approach. The proposed method is parameter-free and only relies on the data. In the next section, the extended EM-EOF method is described. An application to incomplete surface velocity data obtained from cross-correlation of Sentinel-2 images over Fox glacier in New Zealand [11] is presented in section III. Finally, the conclusions are drawn in section IV.

II. THE EXTENDED EM-EOF METHOD

Starting from an appropriate initialization of missing values, the extended EM-EOF method is divided into two stages. At stage 1, the spatio-temporal covariance of the time series is constructed and decomposed into EOF modes. The appropriate number of EOF modes (denoted by R) to reconstruct the time series is estimated by minimizing the root-mean-square error between cross-validated data and the reconstructed field (cross-RMSE). Stage 2 follows an EM-like scheme: during the E step, missing data are estimated given the observed data and the current estimate of the covariance matrix. The M step consists of a minimization of the error between the reconstructed data with a fixed number of EOF modes. This process iteratively converges to a minimum error. Once the convergence is reached, the process starts again with an additional EOF mode. Note that at each iteration, the estimated values are used as an initialization of the missing values for the next iteration.

A. Data organization and covariance estimation

Let X_t be a spatial grid of size $P_x \times P_y$ observed at time $t = 1, \ldots, N$, where each element at position (i, j) is noted $x_{ij}(t), 1 \leq i \leq P_x, 1 \leq j \leq P_y$. All observations of X_t are stacked into a spatio-temporal data matrix $Y = (X_1, X_2, \ldots, X_N)$. Note that in practice each X_t has zero mean, i.e. its spatial mean is removed. Each X_t is augmented into a Hankel-block Hankel (HbH) matrix D_t of size $K_x K_y \times M_x M_y$, with $K_x = (P_x - M_x + 1)$, $K_y = (P_y - M_y + 1)$ and where (M_x, M_y) is a two-dimensional window sliding through each X_t (see Fig. 1):

$$D_t = \begin{pmatrix} H_{1,t} & H_{2,t} & \ldots & H_{M_x,t} \\ H_{2,t} & H_{3,t} & \cdot^{\cdot^{\cdot}} & \vdots \\ \vdots & \cdot^{\cdot^{\cdot}} & \cdot^{\cdot^{\cdot}} & \vdots \\ H_{K_x,t} & \ldots & \ldots & H_{P_x,t} \end{pmatrix} \quad (1)$$

Each matrix $H_{i,t}$ is a $K_y \times M_y$ Hankel matrix defined as:

$$H_{i,t} = \begin{pmatrix} x_{i1}(t) & x_{i2}(t) & \ldots & x_{i,M_y}(t) \\ x_{i2}(t) & x_{i3}(t) & \cdot^{\cdot^{\cdot}} & \vdots \\ \vdots & \cdot^{\cdot^{\cdot}} & \cdot^{\cdot^{\cdot}} & \vdots \\ x_{i,K_y}(t) & \ldots & \ldots & x_{i,P_y}(t) \end{pmatrix} \quad (2)$$

In the following, we note $K = K_x K_y$, $M = M_x M_y$ and $P = P_x P_y$ for the sake of convenience. Similarly to Y, each matrix D_t is stacked into a spatio-temporal matrix $\mathcal{D}$ of size $(K \times NM)$, that is $\mathcal{D} = (D_1, D_2, \ldots, D_N)$.

In reference to multi-channel singular spectral analysis (M-SSA) [6], $\mathcal{D}$ is called the *augmented data matrix*. The

difference here is that each matrix X_t is augmented in space instead of time, so that the original one-dimensional window of length M used in M-SSA is now a two-dimensional window of size $M_x \times M_y$ as in 2D-SSA [10], and the considered augmented matrix is spatio-temporal.

The $NM \times NM$ spatio-temporal *lagged covariance* of $\mathcal{D}$ is given by:

$$\hat{C} = \frac{1}{K} \mathcal{D}^T \mathcal{D} \quad (3)$$

Entrywise, $\hat{C}$ is the sum of the cross-products of the entries of $\mathcal{D}$, given by $\hat{C}_{ij} = \frac{1}{K} \sum_{k=1}^{K} \mathcal{D}_{ki} \mathcal{D}_{kj}$ with $i, j = 1, \ldots, MN$.
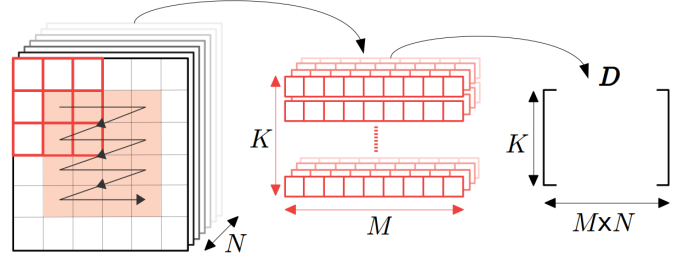

Fig. 1: Data organization (illustration with $M = 9$ and $K = 16$). A M-samples spatial window (in red) is applied to each X_t and translated through K possible positions. Each view of the M-samples window is then vectorized and put into a $K \times M \times N$ intermediary matrix. Finally, sub-dimension $M \times N$ is flattened into K vectors to get matrix $\mathcal{D}$.

B. Decomposition of the covariance

The eigenvalue decomposition (EVD) of matrix $\hat{C}$ yields to:

$$\hat{C} \stackrel{\text{EVD}}{=} \sum_{i=1}^{NM} \lambda_i u_i u_i^T \quad (4)$$

where vectors u_i are the NM *extended* EOFs (EEOFs) of matrix $\mathcal{D}$. Eq. (4) comes from the spectral representation theorem, and each of its terms is called an *EOF mode* [4]. The fraction of total variance explained by EOF mode i is indicated by the value $\lambda_i / \sum_i \lambda_i$: in general, the first EOF modes represent most of the variability of the signal in Y.

To reconstruct Y, one needs to first define the principal components (PC's) a_k with $1 \leq k \leq NM$, which are the projections of the augmented matrix on each EEOF:

$$a_{ik} = \sum_{j=1}^{NM} \mathcal{D}_{ij} u_{jk}, \qquad i = 1, \ldots, K \quad (5)$$

Note that each PC has length K. The augmented matrix can be partially or fully reconstructed by projecting the PC's on the corresponding extended eigenvectors. If A is the $K \times NM$ matrix containing the PC's in its columns and U is the right-eigenvector matrix obtained from the EVD of $\hat{C}$, then the reconstruction takes the form $\hat{\mathcal{D}} = AU$, where each element of $\hat{\mathcal{D}}$ is given by

$$\hat{\mathcal{D}}_{ij} = \sum_{k=1}^{NM} a_{ik} u_{jk} \quad (6)$$

Then, diagonal averaging, called *hankelization*, is applied successively to each matrix $\boldsymbol{H}_{i,t}$ and to each matrix $\boldsymbol{D}_t$, so that we have the following averaging:

$$x_{ij}(t) = \frac{1}{\#\mathcal{A}_j} \sum_{(l,l')\in\mathcal{A}_j} x_{ll'}(t) \tag{7}$$

$$\boldsymbol{H}_{i,t} = \frac{1}{\#\mathcal{B}_i} \sum_{(l,l')\in\mathcal{B}_i} \boldsymbol{H}_{ll',t} \tag{8}$$

with $\mathcal{A}_j = \{(l,l') : 1 \le l \le K_y, 1 \le l' \le M_y, l+l' = j+1\}$, $\mathcal{B}_i = \{(l,l') : 1 \le l \le K_x, 1 \le l' \le M_x, l+l' = i+1\}$ and $\#$ is the cardinality of sets $\mathcal{A}_j$ and $\mathcal{B}_i$.

The reconstructed data matrix, noted $\hat{\boldsymbol{Y}}$, is finally retrieved from $\hat{\mathcal{D}}$ by reversing the process of Fig. 1 (simple one-to-one correspondence). Note that the truncation of Eq. (6) by a number $R \ll MN$ of EEOFs allows to remove the non-significant part of the signal, (e.g. noise). The choice of the appropriate truncation is discussed is the next subsection.

C. Selection of the optimal number of EOF modes

To estimate the optimal number of EOF modes R, the cross-RMSE is used as a metric [4]. Cross-RMSE is the ℓ_2-norm of the difference between a cross-validation data set $\mathcal{Y} \in \boldsymbol{Y}$ and its estimate based on k EEOFs $\hat{\mathcal{Y}}_k$. Cross-RMSE $\{\epsilon_1, \ldots, \epsilon_{MN}\}$ is computed with $\epsilon_k = \frac{1}{MN}||\hat{\mathcal{Y}}_k - \mathcal{Y}||_2$. The optimal number of EOF modes is then found as the one that minimizes the cross-RMSE. As underlined in [4], strong mixing between correlated noise and true signal (e.g. displacement signal) can lead to an over-estimation of the number of EOFs modes, which can be explained by the contamination of cross-validation data by noise. To overcome this issue, a tuning criterion was proposed in [4], which can be limited in the case of degenerate eigenvalues. Degeneracy (close eigenvalue) and/or separation (distant eigenvalue) in the eigenvalue spectrum provides useful information on both signal frequencies distribution and spatio-temporal variability. Degeneracy of eigenvalues makes the interpretation of the corresponding EOFs difficult since any linear combination of these EOFs is also an EOF, which leads to a mixing of the EOFs [7]. Two or multiple consecutive eigenvalues (called multiplet) are degenerate when the uncertainty of an eigenvalue is comparable with or larger than the spacing between this eigenvalue and its closest neighbor. Therefore, to investigate multiplet degeneracy, the uncertainty of eigenvalues must be first estimated. [12] proposed a "rule of thumb" to approximate the eigenvalue uncertainty:

$$\Delta\lambda_k \approx \sqrt{\frac{2}{L^*}}\lambda_k \qquad \Delta\boldsymbol{u}_k \approx \frac{\Delta\lambda_k}{\lambda_j - \lambda_k}\boldsymbol{u}_j \tag{9}$$

where λ_j is the closest eigenvalue from λ_k, $\boldsymbol{u}_j$, $\boldsymbol{u}_k$ are the corresponding eigenvectors, L^* is the number of independent observations in the spatio-temporal sample also called *effective sample size* (named ESS hereafter). The interpretation of Eq. (9) is the following: if the uncertainty of eigenvalue λ_k is close to the difference between this eigenvalue and its closest neighbor, then the corresponding eigenvectors are likely to be contaminated one by each other. This contamination exists

when, for example, two eigenvectors describe together the same spatio-temporal pattern or if the signal is perturbed by correlated noise, which has the effect of "spreading" the variance over the spectrum. To estimate the spatio-temporal ESS L^*, we separate it into two distinct parts such that $L^* = N^*M^*$. N^* corresponds to the temporal ESS and M^* to the spatial ESS. [13] have given an estimation of N^* by $N\left[1 + 2\sum_{k=1}^{N-1}(1 - \frac{k}{N})\rho(k)\right]^{-1}$, where $\rho(k)$ is the autocorrelation of the time series and N is the number of observations in time. This definition holds for a univariate time series of N observations, e.g. a pixel value varying over time. Following this definition, we estimate the spatial ESS M^* within each spatial window of size M by

$$M^* = M\left(1 + 2\nu \sum_{k=1}^{M}(1 - \frac{k}{M})\right)^{-1} \tag{10}$$

where $\nu = \frac{1}{N}\sum_{t=1}^{N} I_t$ is the average spatial autocorrelation and I_t is the Moran's I statistics of spatial field $\boldsymbol{X}_t$.

Based on the estimated uncertainty of eigenvalues given in Eq. (9), a measure of confidence $\mathcal{C}_k$ associated with each eigenvalue λ_k can be computed in the $[0,1]$ interval:

$$\mathcal{C}_k = \frac{\max(\Gamma_k) - \Gamma_k}{\max(\Gamma_k) - \min(\Gamma_k)} \qquad k = 1, \ldots, NM \tag{11}$$

with $\Gamma_k = \log\left(\frac{\Delta\lambda_k}{\lambda_j - \lambda_k}\right)$. $\mathcal{C}_k$ allows to detect degeneracy and/or separation of the eigenvalues in the spectrum of $\mathcal{D}$, which respectively correspond to lower and higher values of $\mathcal{C}_k$. That is, any peak in $\mathcal{C}_k$ coincides with a separation between two eigenvalue multiplets whereas lower "sidepeak" values correspond to degeneracy of a multiplet or close eigenvalues.

To refine the optimal number of EOF modes R previously determined using the cross-RMSE, $\mathcal{C}_k$ is computed for $k = 1, \ldots, MN$. Then, the peaks in $\mathcal{C}_k$ corresponding to the separations in the eigenvalue spectrum are detected. If R corresponds to a peak of $\mathcal{C}_k$, the algorithm stops here. Otherwise, if a subsequent $\mathcal{C}_k$ is high enough (e.g. $\mathcal{C}_k \ge 0.8$), the optimal number is updated so that it matches index k.

D. Determination of the spatial lag M

The choice of M is generally dictated by a trade-off between the amount of information extracted in the window (M should be large) and the number of repetitions of the window within each image (M should be small) [14]. Instead of a single value, a range of M can provide satisfactory results. In this paper, two metrics are proposed to determine the range of M. The first metric is based on the covariance estimation theory, that is, the number of independent samples should be at least twice the number of variables. Thus, the maximum value of M can be determined by solving $K > 2M$. Simple calculations lead approximately to $M < P/6$. The second metric is based on the spatial auto-correlation property of the displacement field. Let τ be the spatial decorrelation decay defined as $\tau = -\frac{\Delta P}{\log r}$, where r is the lag-one auto-correlation and ΔP is the spatial sampling rate, here 1 pixel. Following [6], M can be approximated by $M \simeq P/\tau$. In most cases, r is supposed to be smaller than 0.95, which gives $M > P/20$.

III. Application to glacier surface flow velocity

The extended EM-EOF method is applied to surface velocity data obtained from cross-correlation of Sentinel-2 images over Fox glacier in New Zealand [11]. The data set consists of a time series of 12 velocity fields extending from February to mid-September 2018 (Fig. 2). Each velocity field has a temporal baseline ranging from 10 to 40 days. The grid size of each velocity field is 100×150. All velocity fields contain missing data which correspond to discarded values due to low correlation : their quantity per velocity field varies from 10% to 60%. Missing values are initialized by the spatial mean. The number of cross-validation points, which are randomly chosen, is set to 1% of the observed points per velocity field. The spatial lag is fixed to $M = 225$ (window of size 15×15), which, considering the quantity of points over the glacier, roughly corresponds to the lower limit of the lag.

Results of the reconstruction are shown in Fig. 3, with an estimated optimal number of EOF modes of 13. Fig. 4 shows the scree plot (Fig. 4a), as well as the confidence index $\mathcal{C}_k$ associated with each eigenvalue (Fig. 4b). The estimated number of EOF modes corresponds to a peak in $\mathcal{C}_k$, which coincides to a break in the eigenvalue spectrum. Eigenvalues λ_1 to λ_4 and three multiplets corresponding to sets $\{\lambda_5 - \lambda_7\}, \{\lambda_8 - \lambda_{11}\}$ and $\{\lambda_{12}, \lambda_{13}\}$ are kept in the reconstructed data. Reconstructed surface flows show that seasonal variations are retrieved and similar to the observations in [11]. Velocities reach 1500 m/year in the lower part of the glacier, which is consistent with the maximum speed of 4.5 m/day below the main ice fall of Fox Glacier [15].

Time series of surface velocity over three locations, P1, P2, and P3, are shown in Fig. 5. P1 corresponds to the location picked in [11] and P2 is closer to the glacier central flowline. P3 is located in the lower part of the glacier and its time series contains only one observed value (2018-02-01) due to the rapid surface velocity. Time series at P1 location is complete whereas the one at P2 contains missing values. As P1 and P2 are close to each other, we consider that the seasonal variation only differs by a scale factor over these two points. Thus, the temporal evolution trend over P1 can be used to validate the reconstructed displacement values over P2. Reconstructed values at location P2 are globally consistent with observed values in the time series (inside the error bar in most cases). Reconstruction at location P3 shows that the seasonal trend is retrieved, despite the large amount of missing data. The extended EM-EOF gives improved results compared to the EM-EOF method with a gain of $\simeq 15$ m/year on average in accuracy, especially when data gaps are large (from April to August). This observation highlights the contribution of the exploitation of both spatial and temporal correlation in the reconstruction, as supported by synthetic simulations (Figs. S2-S3 in the supplementary material). The reconstruction also corrects spatial artifacts in the higher part of the displacement (e.g. 2018-08-31/09-19), which is underpinned by simulations (Figs. S1 and S4). Note also that the reconstruction of 2018-07-15 by both EM-EOF and extended EM-EOF is smaller than the observed values. Detailed inspection suggests that this is mainly due to the presence of outliers at the edge of some discontinuous areas in the initial data.

IV. Conclusion

In this paper, an extention of the EM-EOF method [4] is presented for missing data imputation in displacement time series. The temporal covariance matrix is extended to a spatio-temporal covariance by augmenting the data in space. A robust selection of the number of EOF modes based on i) cross-validation and ii) uncertainty analysis of the eigenvalues is also proposed. For the latter, the problem of eigenvalue degeneracy is addressed by extending the rule of thumb of [12] with spatio-temporal sampling, and a measure of confidence associated with each eigenvalue is derived to select the optimal set of EOF modes. In addition, spatial lag range is provided using simple guidelines from both covariance estimation theory and spatial decorrelation. An application to displacement time series over Fox Glacier, New Zealand is presented to show the ability of the proposed method to interpolate short time series of 2D displacement fields with large amount of spatially correlated data gaps. The extended EM-EOF method is able to separate and extract the displacement signal from perturbations even when a few data is available in time. This observation is supported by the retrieval of seasonal variations in the reconstructed surface velocities. The comparison with the EM-EOF method also shows a gain in accuracy. This new tool can help to increase the effective size of a short and incomplete time series: it also goes a step further to meet the need of complete glacier surface velocities for a better knowledge of rheological parameters that control it. In future work, an estimation of the spatio-temporal covariance with adaptive window will be developed in order to avoid potential edge effects at the glacier boundaries.

References

[1] Y. Yan, A. Dehecq, E. Trouve, G. Mauris, N. Gourmelen, and F. Vernier, "Fusion of remotely sensed displacement measurements: Current status and challenges," *IEEE Geosci. Remote Sens. Mag.*, vol. 4, no. 1, pp. 6–25, 2016.

[2] Rémi Prébet, Yajing Yan, Matthias Jauvin, and Emmanuel Trouvé, "A data-adaptative eof based method for displacement signal retrieval from insar displacement measurement time series for decorrelating targets," *IEEE Trans. Geosci. Remote Sens.*, 2019.

[3] Guojie Wang, Damien Garcia, Yi Liu, Richard de Jeu, and A. Johannes Dolman, "A three-dimensional gap filling method for large geophysical datasets: Application to global satellite soil moisture observations," *Environmental Modelling & Software*, vol. 30, pp. 139 – 142, 2012.

[4] Alexandre Hippert-Ferrer, Yajing Yan, and Philippe Bolon, "EM-EOF: gap-filling in incomplete SAR displacement time series," *IEEE Trans. Geosci. Remote Sens.*, 2020, (Accepted).

[5] J. M. Beckers and M. Rixen, "EOF calculations and data filling from incomplete oceanographics datasets.," *J. Atmos. Oceanic Technol.*, vol. 20(12), pp. 1836–1856, 2003.

[6] M. Ghil, M.R. Allen, M. D Dettinger, K. Ide, D. Kondrashov, M.E. Mann, A.W. Robertson, A. Saunders, Y. Tian, F. Varadi, and P. Yiou, "Advanced spectral methods for climatic time series.," *Review of Geophysics*, vol. 40, 1, pp. 1–41, 2002.
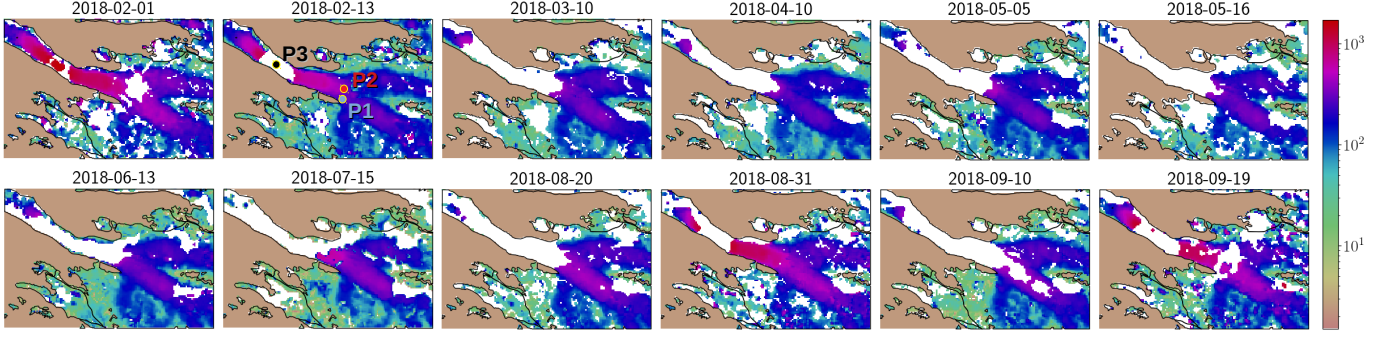
Fig. 2: Time series of surface velocity fields (meters/year) obtained from offset tracking of Sentinel-2 images over Fox Glacier from February to mid-September 2018. Locations P1 and P2 are used for a temporal evolution analysis showed in Fig. 5.
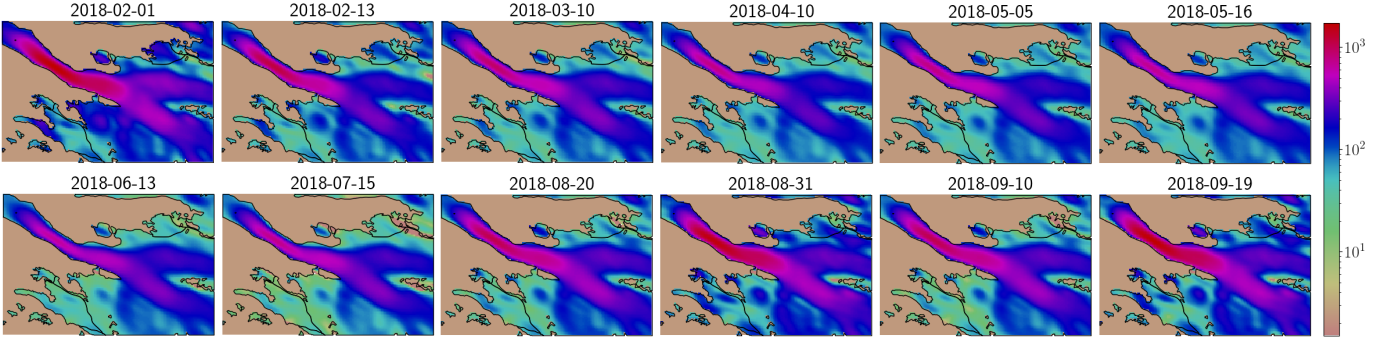

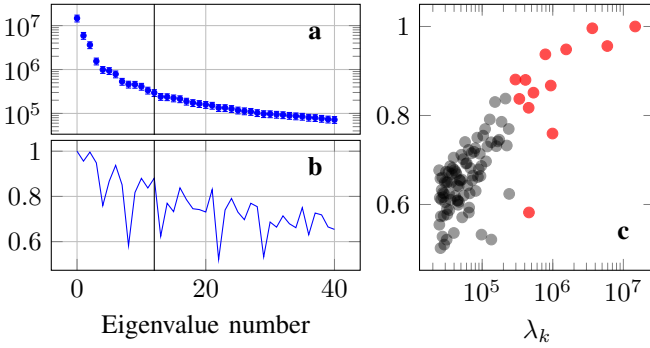Fig. 3: Reconstruction of the time series of velocity fields (meters/year) showed in Fig. 2.

Fig. 4: (a) Eigenvalues λ_k of augmented data matrix $\mathcal{D}$ (first 40 shown) and (b) associated confidence index $\mathcal{C}_k$. The estimated optimal number of EOF modes is 13, which corresponds to a peak in $\mathcal{C}_k$ (black vertical line). (c) shows $\mathcal{C}_k$ versus λ_k. Red marks show eigenvalues corresponding to the selected modes.
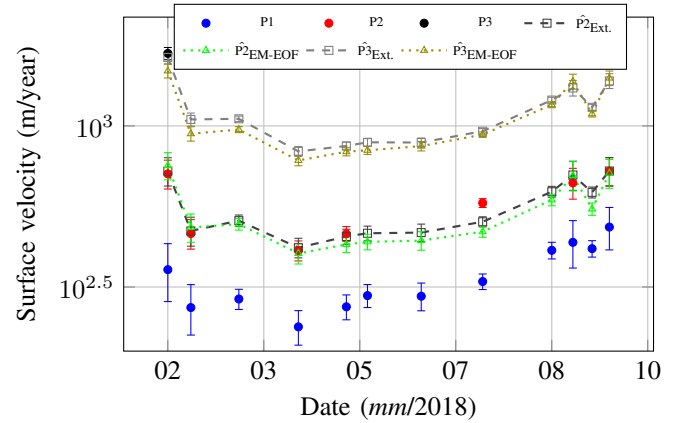
Fig. 5: Time series of glacier surface velocity from February to mid-September 2018 over locations P1, P2, P3 and reconstructed time series over P2 and P3. Errors are from [11].

[7] A. Hannachi, I.T. Jollife, and D.B. Stephenson, "Empirical orthogonal functions and related techniques in atmospheric science: A review.," *Int. J. Climatol.*, vol. 27, pp. 1119–1152, 2007.

[8] D. Kondrashov and M. Ghil, "Spatio-temporal filling of missing points in geophysical data sets," *Nonlinear Processes Geophys.*, vol. 13, pp. 151–159, 2006.

[9] Chang Xu, "Reconstruction of gappy GPS coordinate time series using empirical orthogonal functions," *J. Geophys. Res. Solid Earth*, vol. 121, pp. 9020–9033, 2016.

[10] N.E. Golyandina and K.D. Usevich, "2d-extension of singular spectrum analysis: Algorithm and elements of theory," *Matrix Methods: Theory, Algorithms and Applications*, pp. 449–473, 2010.

[11] Romain Millan, Jérémie Mouginot, Antoine Rabatel, Seongsu Jeong, Diego Cusicanqui, Anna Derkacheva, and Mondher Chekki, "Mapping surface flow velocity of glaciers at regional scale using a multiple sensors approach," *Remote Sensing*, vol. 11, no. 21, 2019.

[12] Gerald R. North, Thomas L. Bell, Robert F. Cahalan, and Fanthune J. Moeng, "Sampling errors in the estimation of empirical orthogonal functions," *Monthly Weather Review*, vol. 110, pp. 699–706, 1982.

[13] H. J. Thiébaux and F. W. Zwiers, "The interpretation and estimation of effective sample size," *J. Climate Appl. Meteor.*, vol. 23, no. 5, pp. 800–811, 1984.

[14] Andreas Groth and Michael Ghil, "Monte carlo singular spectrum analysis (SSA) revisited: Detecting oscillator clusters in multivariate datasets," *J. Climate*, vol. 28, no. 19, pp. 7873–7893, 2015.

[15] Andreas Kääb, Solveig H. Winsvold, Bas Altena, Christopher Nuth, Thomas Nagler, and Jan Wuite, "Glacier remote sensing using sentinel-2. part i: Radiometric and geometric performance, and application to ice velocity," *Remote Sensing*, vol. 8, no. 7, 2016.